AIAA 80-1794R

Hardware Demonstration of Flexible Beam Control

David B. Schaechter*
Jet Propulsion Laboratory, California Institute of Technology, Pasadena, Calif.

An experiment employing a pinned-free flexible beam has been constructed to demonstrate and verify several facets of the control of flexible structures. The desired features of the experiment are to demonstrate active shape control, active dynamic control, adaptive control, various control law design approaches, and associated hardware requirements and mechanization difficulties. This paper contains the analytical work performed in support of the facility development, the final design specifications, control law synthesis, and some preliminary results.

Nomenclature

A = amplitude
A = state weighting matrix
B = control weighting matrix
C = control gain matrix
E = Young's modulus
f = nonlinear function
f = force per unit length
f_n = nth modal force
F = concentrated force
F = continuous system dynamics matrix
g = acceleration of gravity
G = continuous system control distribution matrix
H = continuous system observation matrix
I = moment of inertia
J = scalar performance index
J_0 = Bessel function of zero order
k = stage variable
K = measurement gain matrix
L = length
m = number of controls
n = number of states
M = total mass
p = number of sensors
q = modal amplitude
Q = spectral density of process noise
R = spectral density of measurement noise
t = time variable
T = sample period
T = torque
T_c = command torque
u = continuous control
u_k = control vector at stage k
v = measurement disturbance
w = process disturbance
x = running spatial variable
x = continuous state vector
x_k = state vector at stage k
y = deflection of beam
z = continuous measurement vector
z_k = measurement vector at stage k
Γ = continuous system process noise distribution matrix
δ = Dirac delta function
ϵ = small parameter
ξ = normalized running spatial variable
ξ = damping ratio
ξ_0 = specific value of normalized spatial variable
ξ_n = damping ratio of nth mode
λ_n = nth eigenvalue
ρ = mass per unit length
ϕ_n = nth eigenvector
Φ = state transition matrix
ψ = time dependent phase variable
ω_n = nth natural frequency
E = expected value operator
$(\ )_{\max}$ = maximum value
$(\dot{\ })$ = time derivative
$(\ )^T$ = vector transpose
$(\ )_{\text{avg}}$ = averaged value

Presented as Paper 80-1794 at the AIAA Guidance and Control Conference, Danvers, Mass., Aug. 6-8, 1980; submitted Oct. 24, 1980; revision received April 29, 1981. This paper is declared a work of the U.S. Government and therefore is in the public domain.

*Member of Technical Staff. Member AIAA.

I. Introduction

THE Large Space System Technology (LSST) Flexible Beam Experiment was constructed to demonstrate and verify several facets of the control of large flexible space structures. The desired features of this experiment were to demonstrate: 1) active shape control, 2) active dynamic control, 3) various control law design approaches, 4) adaptive control, and 5) microprocessor control capability.

This paper describes, in detail, the analytical work performed in support of the facility development, the final design specifications, control law synthesis, and some preliminary results.

II. Flexible Beam Analysis

Configuration

The flexible beam was chosen for this experiment for being a simple, continuous structure with many of the dynamic characteristics that are representative of general large space structures, including, infinitely many vibration modes, a rigid-body mode, and many "low"-frequency vibration modes.

The selection of the flexible beam also resulted in some minor limitations. The flexible beam does not have repeated eigenvalues, however, by orthogonality of the corresponding eigenvectors, these modes may be distinguished spatially, if not by frequency domain methods. Secondly, totally free boundary conditions are not possible in a ground based experiment. Two beam support configurations, which replace the rigid-body mode with a low-frequency pendulum mode, were considered as alternatives and are shown in Fig. 1. Figure 1a shows the beam supported by several cables in the horizontal direction, and Fig. 1b shows the beam hanging vertically from a pinned support. Although the configuration in Fig. 1a more closely approximates the totally free boundary conditions, the complexity of distributing the weight of the beam uniformly, and the difficulty with constraining the unwanted degrees of freedom in Fig. 1a, resulted in selection of the pinned-free hanging beam of Fig. 1b as the final configuration.

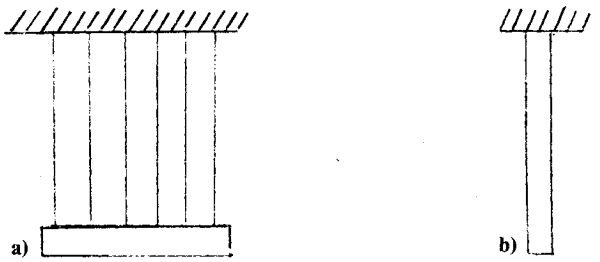

Fig. 1 Beam support configurations.

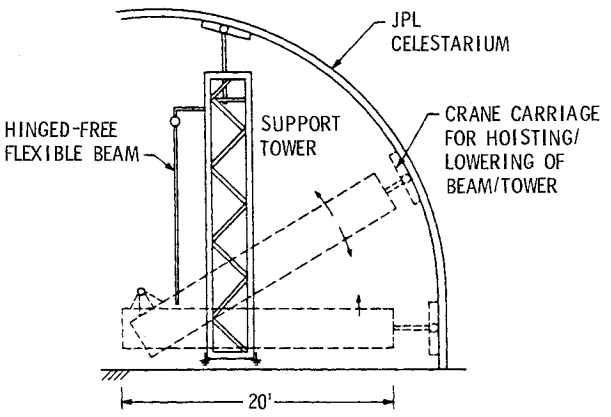

Fig. 2 Beam support structure.

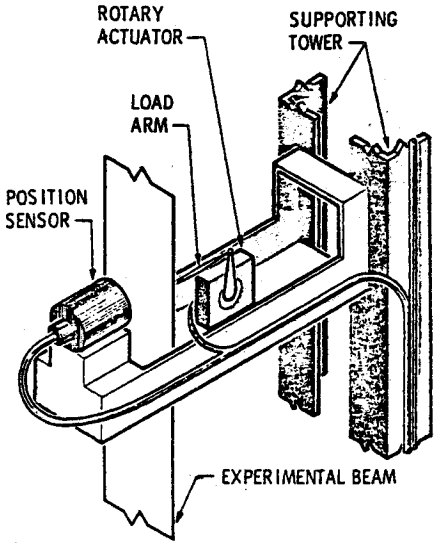

Fig. 3 Sensor/actuator mounting bracket.

One further compromise had to be made in the sensing/actuation phase of this experiment. A totally free space structure is constrained to sense with respect to (and react against) itself, or inertial space. Because the major objectives of this experiment are to demonstrate control technology, and not sensor/actuator technology, sensing and actuation of the beam are both performed with respect to an external frame.

A schematic of the beam support structure (tower) as it is being erected is shown in Fig. 2. The tower is constructed of aluminum angles and is 20 ft tall, 2 ft deep in the stiff direction, and 1 ft deep in the compliant direction. The weight of the tower is 200 lb. With the sensor/actuator mounting brackets (Fig. 3), beam, sensors, actuators, and electronics, the total weight is about 300 lb.

Shake tests were performed on the tower to determine its resonances, and if they might interact with the control of the flexible beam. The results are given in order of increasing frequency in Table 1.

Table 1 Tower resonances

Frequency, Hz	Mode	Direction
6	cantilever	compliant
10	cantilever	stiff
27	pinned-free	compliant
35	pinned-free	stiff
45	free-free	compliant
63	free-free	stiff

For the final configuration, only the natural frequencies in the stiff direction are of interest, because there is very little coupling between the perpendicular directions.

A schematic of the sensor/actuator mounting bracket is shown in Fig. 3. Either the sensor or actuator, or both, may be mounted on a single bracket, and the brackets may be mounted at any of the stations located at 6 in. intervals along the beam.

Dynamic Analysis

A dynamic model of the hanging, pinned-free beam is required for control system design. For more complex structures, a NASTRAN model is generally used for obtaining the natural frequencies and mode shapes. However, for the simple beam, closed-form analytical solutions can be derived.

Temporarily setting aside the effects of the beam being in tension due to gravity, the partial differential equation of motion for the elastic beam with constant mass and stiffness per unit length, and the appropriate boundary conditions are

$$\rho\frac{\partial^2 y}{\partial t^2}+EI\frac{\partial^4 y}{\partial x^4}=f$$

$$y(0,t)=0 \qquad \frac{\partial^2 y}{\partial x^2}(L,t)=0 \qquad (1)$$

$$\frac{\partial^2 y}{\partial x^2}(0,t)=0 \qquad \frac{\partial^3 y}{\partial x^3}(L,t)=0$$

It is straightforward to show by assuming an eigenvector decomposition of the solution that the eigenvalues and normalized eigenvectors are

$$\phi_0(\xi)=\sqrt{3/L}\,\xi \qquad \omega_0=0 \qquad (2)$$

$$\phi_n(\xi)=\sqrt{\frac{(2/L)\cosh^2\lambda_n\cos^2\lambda_n}{\cosh^2\lambda_n-\cos^2\lambda_n}}\left[\frac{\sinh\lambda_n\xi}{\cosh\lambda_n}+\frac{\sin\lambda_n\xi}{\cos\lambda_n}\right]$$

where

$$\omega_n^2=EI\lambda_n^4/\rho L^4 \qquad \tanh\lambda_n=\tan\lambda_n \qquad \xi=x/L$$

Using an asymptotic approximation (good for $n\geq 1$) for Eq. (2)

$$\phi_0(\xi)=\sqrt{3/L}\xi \qquad \omega_0=0$$

$$\phi_n(\xi)\sim\frac{1}{\sqrt{L}}\left[\frac{\sinh\lambda_n\xi}{\cosh\lambda_n}+\frac{\sin\lambda_n\xi}{\cos\lambda_n}\right] \qquad \lambda_n\sim\frac{(4n+1)\pi}{4}$$

$$(n=1,2,3,\ldots) \qquad (3)$$

The dynamic equations for the modal amplitudes, q_n, become

$$\ddot{q}_n+\omega_n^2 q_n=\int_0^l\frac{\phi_n(\xi)f(\xi)\,d\xi}{\rho}\triangleq f_n \qquad (n=0,1,2,\ldots) \qquad (4)$$

For the specific case that $f(\xi,t)=F(t)\delta(\xi_0)$, i.e., a spatially concentrated force applied at $\xi=\xi_0$,

$$f_n = (F/M)\phi_n(g_0) \tag{5}$$

A graph of the first five mode shapes is shown in Fig. 4.

The rigid body motion of Fig. 4a is a zero-frequency eigenvalue. Of course, for the pinned-free beam hanging under the influence of gravity, no such mode exists. Rather than being a zero frequency, rigid body mode, the actual dynamics is a low frequency, pendulum-like behavior. In fact, gravity interacts with all of the modes to some degree. To determine which behavior (tension or elastic) dominates the various modes, an independent dynamic analysis of a hanging free string will be performed.

The partial differential equation of motion for a hanging string, with its boundary conditions is

$$\rho\frac{\partial^2 y}{\partial t^2} = \frac{\partial}{\partial x}\rho g x\frac{\partial y}{\partial x} \qquad y(0) = \text{finite} \qquad y(L) = 0 \tag{6}$$

The solution to Eq. (6) is given by

$$\phi_n = J_0(\omega_n\sqrt{4x/g})$$

where

$$J_0(2\omega_n\sqrt{L/g}) = 0 \tag{7}$$

Again, an asymptotic approximation to the eigenvalues can be obtained

$$\omega_n^2 \sim \frac{g}{2L}\frac{(n-\frac{1}{4})^2\pi^2}{2} \tag{8}$$

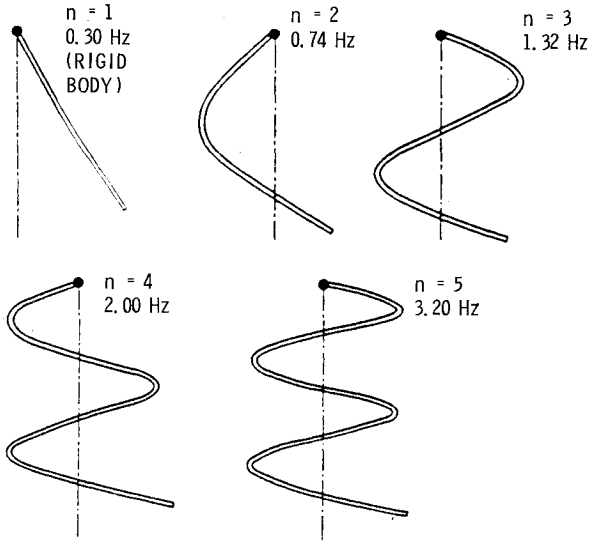

Fig. 4 Flexible beam mode shapes.

The first five mode shapes are almost identical to those shown in Fig. 4.

If the true mode shapes of the exact system are obtained from Eq. (9)

$$\rho\frac{\partial^2 y}{\partial t^2} + EI\frac{\partial^4 y}{\partial x^4} - \rho g\frac{\partial}{\partial x}(L-x)\frac{\partial y}{\partial x} = f \tag{9}$$

it can be shown that the square of the exact eigenvalues are approximately the sum of the squares of the string and the beam frequencies, with the largest error occurring when the two frequencies are equal. For the beam parameters in Table 2, Table 3 gives the string frequencies, the beam frequencies, the combined frequencies, and the frequencies of the beam as determined experimentally.

As can be seen in Table 3, or by Eqs. (3) and (8), the beam natural frequencies increase with the square of the mode number, while the string natural frequencies increase linearly with the mode number. Therefore, for sufficiently high mode numbers, the behavior of the hanging beam is beam-like.

The beam parameters used in the final experiment are those given in Table 2. Essentially, the beam parameters were chosen to yield frequencies that were low enough to be easily observed, and to allow sufficient time for control calculations to be performed in a microprocessor. Stainless steel was chosen for its decreased sensitivity to external disturbances (such as air resistance and magnetic forces).

III. Bridging the Dynamics/Control Gap

Before beginning the control system design phase, some additional analysis is required. Such questions as: How many modes can be observed? How many modes can be controlled? and How much computation is required? will be addressed in the following sections.

Sensors

In order to determine what can be observed with a sensor, some "'typical" motion of the beam must be postulated. The typical motion considered here is the response of the beam to an impulsive, concentrated force $F\delta(t_0)\ \delta(L)$, applied to the free end of the beam. It is easy to show

$$q_{n\,\max} = F/M\omega_n \qquad \dot{q}_{n\,\max} = F/M \tag{10}$$

Table 2 Beam characteristics

Material	stainless steel
Length	150 in.
Width	6 in.
Thickness	1/32 in.
Linear density	0.638 lb/ft
Elastic modulus	30×10^6 lb/in.^{2}
Area moment	1.526×10^{-5} in.^{4}

Table 3 Beam natural frequencies (Hz)

	Analytical solution			Experimental determination		
Mode no.	String	Beam	Combined	No. of cycles	Time, s	Frequency
0	0.30	0.00	0.30	23	76.0	0.30
1	0.70	0.28	0.75	34	46.2	0.74
2	1.10	0.92	1.43	38	28.9	1.32
3	1.50	1.94	2.45	30	15.0	2.00
4	1.91	3.22	3.74			
5	2.31	5.72	6.16			
6	2.71	6.99	7.50			
7	3.11	9.39	9.89			
8	3.51	12.2	12.7			
9	3.91	15.3	15.8			
10	4.31	18.8	19.3			

Table 4 Observable modes vs position sensor resolution

No. of modes	Sensor resolution
3	10%
10	1%
31	0.1%
100	0.01%

and that these maxima occur at the free end of the beam. With a position sensor configured so the lowest frequency mode exercises the full sensor range, and recalling that ω_n increases as n^2, a table of the number of modes that are visible vs sensor resolution can be constructed (Table 4).

Both an optical position sensor, and an eddy current position sensor reached the final selection phase. Many other possibilities were eliminated by the requirement of minimum sensor interaction with the beam dynamics. In order to minimize the effects of external disturbances, the developmental period, and the final cost, an eddy current sensor, made by Kaman Science Corporation, was selected. Its output is a dc voltage between ± 1 V, and the unit has an accuracy of 0.001 in., according to the manufacturer's specifications. The sensor support bracket was changed to lucite construction in order to locate all metal objects (except the beam) sufficiently far from the sensor.

Actuators

The purpose of this control experiment is to demonstrate shape control and dynamic vibration control. Since the desired shapes are relatively smooth, and the associated bandwidth of the shape control system is low, the maximum actuation forces are dictated by the requirements for dynamic control. In order to assess what magnitude of control effort is required, some typical motion of the controlled beam must be assumed. For actuator sizing, it is assumed that the function of the control system is to add damping to the various modes, in which case

$$F/M = -2\xi_n\omega_n\dot{q}_n \qquad \ddot{q}_n + \omega_n^2 q_n = F/M \tag{11}$$

If F is small, a good approximation to $q_n(t)$ is simply

$$q_n = A\sin(\omega_n t + \phi) \qquad \dot{q}_n = A\omega_n\cos(\omega_n t + \phi) \tag{12}$$

and so the root mean square (rms) value of F can be computed as

$$F_{\text{rms}} \sim \sqrt{2}\xi_n\omega_n^2 AM \tag{13}$$

Assuming, as before, a 1 in. amplitude of the first mode, and that the modal amplitudes decrease as $1/\omega_n$

$$F_{\text{rms}} \sim \sqrt{2}\xi_n\omega_n M = 0.0292\xi_n\omega_n \tag{14}$$

where F is in pounds.

As an example, to add 10% damping to the sixth mode will require 0.27 lb force in an rms sense.

The final actuator selection was a brushless dc torque motor manufactured by Aeroflex Laboratories, Inc. With a 3 in. moment arm and the appropriate mechanical linkages, the actuator has the capability of applying 5 oz of force to the beam for a maximum 1 amp input, according to the manufacturer's specifications.

Microcomputer

The purpose of the microcomputer in the control loop is to sample the sensors, pass this sampled data through a digital filter, and send the filtered data to the actuators. Assuming a general format for the digital filter,

Table 5 Computation time requirements

Controlled modes	Software multiply (@1 ms/mult), ms	Hardware multiply (@0.1 ms/mult), ms	Period of nth mode, ms
1	4	0.4	3300
2	16	1.6	700
3	36	3.6	409
4	64	6.4	268
5	100	10.0	162
6	144	14.4	133
7	196	19.6	101
8	256	25.6	78
9	324	32.4	63

$$x_{k+1} = \Phi x_k + Kz_k \qquad u_k = Cx_k \tag{15}$$

The amount of computation is roughly $n^2 + np + nm$ multiplications. For the state vector larger than either the number of sensors or actuators, the amount of computation is governed by the n^2 term. Currently available eight-bit microprocessors are capable of performing one fixed-point double precision software multiply in 1 ms, and one hardware floating point multiply in 100 μs. As such, Table 5 can be constructed illustrating the time required to control a given number of modes.

Due to the limitation imposed by the sampling theorem (i.e., sample two or more times per cycle) the maximum number of controlled modes with software arithmetic is four, and the maximum number using hardware arithmetic is eight.

The microcomputer chosen for the control function is the SYM-1 by Synertek System Corporation. It is based on the 6502 microprocessor, and has provisions for 4 K of random access memory (RAM), and 6 K of read only memory (ROM). Additionally, a KIMSI Interface/Motherboard, by Forethought Products, has been added for interfacing directly to S-100 products, specifically the digital to analog converters, and the hardware arithmetic.

Sensor sampling is performed under computer control. The twelve-bit analog-to-digital (A/D) conversion is a successive approximation technique performed in software, with the use of a Vector Graphic Precision Analog Interface Board (PAIB). Similarly, the twelve-bit digital-to-analog (D/A) conversion is performed in hardware on the PAIB.

Microcomputer Interfaces

Sensor buffer/amplifiers were used between the sensor output and the computer. The circuit has a high-input impedance, and eliminates high-frequency noise and dc offsets. The scale factor from position to voltage at the A/D converter is 5 V/in. The sensor bandwidth is greater than 30 Hz.

The actuator driver presents a high input impedance to the microcomputer D/A converter, and eliminates the high frequency D/A conversion noise and dc offsets from the actuator command. Current feedback is used to eliminate the inductive effects of the torquer. The scale factor from the force applied to the beam to the D/A voltage output is 1 oz/V. The actuator bandwidth is greater than 30 Hz.

Software Development

Software has been developed to implement the general digital filter discussed in the section on microcomputers. The entire program resides in 2516 erasable programmable ROM by Texas Instruments, and is located on the computer. When the software is initiated, the computer samples the sensors, updates the state estimate, and outputs the control. Data for the program is loaded into RAM and consists of Φ, C, K, and

Table 6 System nonlinearities

Nonlinearity	Functional form
Additional mass/stiffness	$\epsilon\delta(x_0)$
Finite transducer size	$\frac{1}{\epsilon}\int_{x_0-\epsilon/2}^{x_0+\epsilon/2} y(x)\,dx$
Aerodynamic drag	$\epsilon\dot{q}_n\lvert\dot{q}_n\rvert$
Angle dependent torque	$T=T_c(1-\epsilon q_n)$
Nonlinear stiffness	$T=\epsilon q_n^3$
Nonlinear damping	$T=\epsilon\dot{q}_n^3$

Table 7 Effects of nonlinearities

Nonlinearity	Effect on ω	Effect on ξ	$\lvert\epsilon\rvert$	Major effect
Aerodynamic drag	0	$\frac{4\epsilon}{3\pi}A$	0.02	$\xi_0=0.8\%$
Angle dependent torque	0	0	0.5	none
Nonlinear stiffness	$\frac{-\epsilon\omega_n}{16}$	0	<0.01	none
Nonlinear damping	0	$\frac{\epsilon\xi}{8}$	<0.01	none

the dimensions of these matrices. The exact sample period T (in ms) is given by

$$T=0.983n^2+0.963np+0.963nm+0.258n$$
$$+0.154m+0.597p+0.010m^2+0.725$$

IV. System Nonlinearities

Although the analysis of the control of the flexible beam has used linear theory, system nonlinearities appeared throughout the design process. It was required to obtain some estimate of the effects of these nonlinearities in order to decide if an alternate design approach would be required, or if the small nonlinearity could be tolerated. The nonlinearities considered are found in Table 6.

The additional mass and stiffness of the beam were caused primarily as a result of drilling holes in the beam and mounting additional components on the beam. These effects were minimized by drilling 080 holes in the beam for mounting the actuators, and using linkages from the torquer to the beam, which added only an additional 3 g to the beam. The design requirement was to keep the total mass and stiffness changes of the beam to less than 3% variation from the original beam.

The finite transducer size (3 in. diam) resulted in an integrated displacement measurement rather than the displacement of a single point. So

$$z=\frac{1}{\epsilon}\int_{x_0-\epsilon/2}^{x_0+\epsilon/2} y(x)\,dx=\frac{1}{\epsilon}\int_{x_0-\epsilon/2}^{x_0+\epsilon/2}\left[y(x_0)+\frac{\partial y}{\partial y}(x-x_0)\right.$$
$$\left.+\frac{\partial^2 y}{\partial x^2}\frac{(x-x_0)^2}{2}+\ldots\right]dx$$

$$z=y(x_0)+\frac{\epsilon^2}{2}\frac{\partial^2 y(x_0)}{\partial x^2}+\ldots \tag{16}$$

There is no first-order change in the sensor output due to the integrated effect.

The remaining nonlinearities were analyzed using the averaging perturbation method below. The effects of a small nonlinearity are modeled as

$$\ddot{q}_n+\omega_n^2 q_n=\epsilon f(q_n,\dot{q}_n) \tag{17}$$

Assuming that the perturbed solution is of the form

$$q_n=A\sin(\omega_n t+\phi)=A\sin\psi$$

and that

$$\dot{q}_n=A\omega_n\cos\psi \tag{18}$$

then it is straightforward to show

$$(\dot{A})_{\text{avg}}=\left[\frac{\cos\psi\, f}{\omega_n}\right]_{\text{avg}}\qquad(\dot{\phi})_{\text{avg}}=\left[\frac{-\sin\psi\, f}{A\omega_n}\right]_{\text{avg}} \tag{19}$$

The averaged amplitude rate of change may be looked upon as an equivalent change in the linear damping ratio, ξ; and the averaged phase rate of change may be looked upon as an equivalent change in the linear natural frequency, ω_n.

The results are given in Table 7.

All of the nonlinearities considered were tolerable without system redesign.

V. Control Law Design

A variety of control laws may be implemented using the general software discussed in the section on microcomputers. The particular approach used in the initial control law design (and the example presented here), is an implementation of a discrete Kalman filter using a sixth order estimator.

The controller is based on the discretized version of the following continuous system

$$\dot{x}=Fx+Gu+\Gamma\omega\qquad u=Cx\qquad z=Hx+v \tag{20}$$

where

$$x^T=[q_0,\dot{q}_0,q_1,\dot{q}_1,q_2,\dot{q}_2]$$

$$F=\begin{bmatrix}0&-1&0&0&0&0\\3.55&0&0&-0&0&0\\0&0&0&-1&0&0\\0&0&21.60&0&0&0\\0&0&0&0&0&-1\\0&0&0&0&68.72&0\end{bmatrix}$$

With a single position sensor and a single force actuator at the free end

$$H=[1,\ 0\ 1\ 0\ 1\ 0]\qquad G^T=\Gamma^T=[0\ 0.18\ 0\ 0.18\ 0\ 0.18]$$

The control gains, C, and the estimator gains K are determined by minimizing the appropriate performance index J. In the case of the control problem

$$J=\int_0^\infty (x^TAx+u^TBu)\,dt$$

and for this particular example

$$A=\begin{bmatrix}1&&&&&\\&0&&&&0\\&&1&&&\\&&&0&&\\0&&&&1&\\&&&&&0\end{bmatrix}\qquad B=0.0025$$

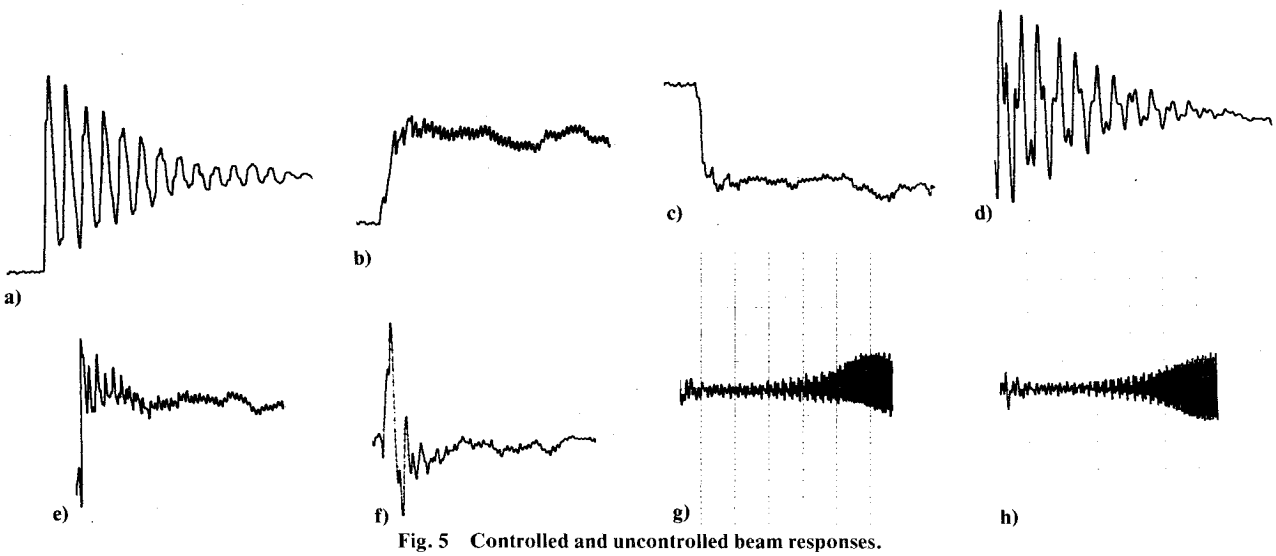

Fig. 5 Controlled and uncontrolled beam responses.

and for the estimation problem

$$J=\int_0^\infty (w^TQ^{-1}w+v^TR^{-1}v)\,dt$$

and for this particular example

$$Q=E(ww^T)=10^{-4}(\text{m/s}^2)^2\text{-s} \qquad R=E(vv^T)=10^{-6}\text{m}^2\text{-s}$$

For a six state estimator, one control, and one sensor, $T=0.049978$ s.

Using a discrete optimal system synthesis (DOPTSYS)[1] algorithm, the following results are obtained.

$$\Phi=\begin{bmatrix} 0.950 & 0.047 & -0.045 & -0.000 & -0.044 & -0.000 \\ -0.251 & 0.910 & -0.085 & -0.033 & -0.053 & -0.019 \\ -0.019 & -0.002 & 0.953 & 0.048 & -0.018 & -0.000 \\ -0.064 & -0.084 & -1.144 & 0.939 & -0.044 & -0.019 \\ -0.011 & -0.002 & -0.011 & -0.000 & 0.904 & 0.048 \\ -0.059 & -0.082 & -0.068 & -0.032 & -3.374 & 0.896 \end{bmatrix}$$

$$K=\begin{bmatrix} 0.0438 \\ 0.0265 \\ 0.0183 \\ 0.0165 \\ 0.0103 \\ 0.0110 \end{bmatrix} \qquad C^T=\begin{bmatrix} -5.3744 \\ -9.4553 \\ -6.5416 \\ -3.7488 \\ -3.0469 \\ -2.2154 \end{bmatrix}$$

and the equivalent frequency domain eigenvalues of the closed-loop system are given by $-0.85\pm2.07j$, $-0.38\pm4.66j$, $-0.21\pm8.29j$, $\xi_0=0.38$, $\xi_1=0.082$, $\xi_2=0.025$.

These matrices are converted to the sixteen-bit fixed point format used by the microcomputer, and are loaded into the controller as data.

The results for this controller can be found in Fig. 5. Figure 5 contains the uncontrolled and controlled responses to both a position initial condition error, and to an impulse force input.

Figure 5a shows the open-loop response to an initial position error. The majority of the response is the lowest frequency, pendulum mode. It has an open-loop damping ratio of ~2%.

Figure 5b shows the closed-loop response to the same input as in Fig. 5a using the controller described previously. Notice the much faster decay rate of the closed loop system. The corresponding control force applied to the beam is shown in Fig. 5c.

It is now possible to partially verify the control analysis. The predicted closed-loop damping ratio for the low frequency mode is 0.38. Using the maximum overshoot of the closed-loop position response for determining the closed-loop damping ratio, the closed-loop damping ratio of 0.40 is experimentally obtained.

Figures 5d-f show analogous responses of the beam to an impulse force disturbance applied at the free end.

One additional feature present in the closed-loop responses in Fig. 5 is the high frequency oscillation appearing at the tail of each plot. This phenomena is due to control/observation spillover into the first unmodeled mode at 2 Hz.

By decreasing the cost of the squared control, B, to 0.0002, this unmodeled mode is driven unstable. In this case, the control and observation spillover is sufficient to overcome the open loop damping of a higher frequency mode and produce the instability. These results are shown in Fig. 5g, the free-end response, and Fig. 5h, the control input.

VI. Conclusions and Future Work

This paper documents the analysis, construction, use, and initial results of the Large Space System Technology (LSST) flexible beam control experiment. The major accomplishment to date has been the development of a workable facility for evaluating the control of flexible structures. Initial closed-loop results have been obtained for a sixth-order dynamic controller, designed using a quadratic performance index, colocated sensors and actuators, and a perfect dynamic model. Future work will eliminate the need for many of the qualifiers in the previous statement. The effects of imperfect models, noncolocated sensors and actuators, shape controllers, high-order estimators, and control design approaches other than the standard quadratic performance index will be studied, using the completed flexible structure facility as an integral portion of this work.

Acknowledgments

Any development such as this requires a team effort. Steve Gunter, George Hotz, Ed Kan, Mark Nelson, Gary Parker, Jeff Schroeder, and Eldred Tubbs all deserve recognition for being vital parts of this team. The research described in this paper was carried out by the Jet Propulsion Laboratory, California Institute of Technology, under NASA Contract No. NAS7-100.

References

[1] Powell, J.D., "Notes on Using Disc for Discrete Control and Filter Synthesis," Lecture Notes, Stanford University, Spring 1977.